

A&A manuscript no. (will be inserted by hand later)
Your thesaurus codes are: 07.19.1

The cluster of galaxies Abell 970. ^{*}

L. Sodré Jr.¹, D. Proust², H. V. Capelato³, G. B. Lima Neto¹, H. Cuevas⁴,
H. Quintana⁵, and P. Fouqué⁶

¹ Departamento de Astronomia do IAG/USP, Av. Miguel Stefano 4200, 04301-904, São Paulo, Brazil

email: laerte@iagusp.usp.br, gastao@iagusp.usp.br

² Observatoire de Paris - Section de Meudon, DAEC, F92195 MEUDON CEDEX, France

email: Dominique.Proust@obspm.fr

³ Divisão de Astrofísica INPE/MCT, 12225-010, Sao José dos Campos, Brazil

email: hugo@das.inpe.br

⁴ Departamento de Física, Universidad de La Serena, Benavente 980, La Serena, Chile

email: hcuevas@ns.df.uls.cl

⁵ Departamento de Astronomia y Astrofísica, Pontificia Universidad Católica de Chile, Casilla 104, Santiago 22, Chile

email: hquintan@astro.puc.cl

⁶ European Southern Observatory, Casilla 19001, Santiago 19, Chile

email: pfouque@eso.org

Received date; accepted date

Abstract. We present a dynamical analysis of the galaxy cluster Abell 970 based on a new set of radial velocities measured at ESO, Pic du Midi and Haute-Provence observatories. Our analysis indicates that this cluster has a substructure and is out of dynamical equilibrium. This conclusion is also supported by differences in the positions of the peaks of the surface density distribution and X-ray emission, as well as by the evidence of a large scale velocity gradient in the cluster. We also found a discrepancy between the masses inferred with the virial theorem and with the X-ray emission, what is expected if the galaxies and the gas inside the cluster are not in hydrostatic equilibrium. Abell 970 has a modest cooling flow, as is expected if it is out of equilibrium as suggested by Allen (1998). We propose that cooling flows may have an intermittent behavior, with phases of massive cooling flows being followed by phases without significant cooling flows after the accretion of a galaxy group massive enough to disrupt the dynamical equilibrium in

Send offprint requests to: D. Proust

^{*} based on observations made at ESO, La Silla (Chile), Haute-Provence and Pic du Midi Observatories (France)

the center of the clusters. A massive cooling flow will be established again, after a new equilibrium is achieved.

Key words: 11.03.01; 11.03.4 Abell 970; 11.04.1; 12.12.1; 13.25.3

1. Introduction

In the present accepted paradigm of structure formation, small structures are the first to collapse, merging then hierarchically to build larger objects. In this framework, clusters of galaxies, the largest (nearly) virialized structures, may be accreting galaxies and/or ‘dark haloes’ even at $z = 0$ (e.g. Lanzoni et al. 2000). Therefore, the study of galaxy clusters may offer important pieces of information for observational cosmology, because cluster properties depend on cosmological parameters and can be used to constrain cosmological scenarios. For instance, the cluster mass function, which may be described by the Press–Schechter formalism (Press & Schechter 1974), depends on the density parameter Ω and on the power spectrum amplitude and shape parameter (e.g., Lacey & Cole 1994, Bahcall & Fan 1998). Also, the morphological and dynamical state of clusters allow us to infer their history and, again, to constrain cosmological theories of large scale structure formation (e.g., Kauffmann et al. 1999).

The mass of a cluster may be estimated by several methods: the optical virial mass, from the positions and radial velocities of the cluster galaxies; the X-ray mass, from the X-ray emission of the hot intracluster gas; the gravitational lensing mass, from the distortions produced on background object images by the gravitational field of the cluster. However, discrepancy between these estimators are often found (e.g., Mushotzky et al. 1995, Girardi et al. 1998, Wu et al. 1998). Virial mass estimates rely on the assumption of dynamical equilibrium. X-ray mass estimates also depend on the dynamical equilibrium hypothesis and on the still not well constrained intra-cluster gas temperature gradient (Irwing et al. 1999). Finally, mass estimates based on gravitational lensing are considered more reliable than the others (e.g., Mellier 1999) because they are completely independent of the dynamical status of the cluster, and their discrepancies with other methods may be due to non-equilibrium effects in the central region of the clusters (Allen 1998).

An important source of departure from equilibrium (that may affect mass estimates) are the substructures. Their very existence supports the current view that clusters grow hierarcally by accreting nearby groups and galaxies. Note that even the frequency and degree of clumpiness in the central regions of the clusters depends on the cosmology (e.g., Richstone, Loeb & Turner 1992). In many cases substructures are loosely bound and can survive only a few crossing time in the hostile environment of rich clusters. However, they seem to be very common in present day clusters. A recent estimate by Kolokotronis

et al. (2000) indicates that at least 45% of rich clusters present optical substructures. Substructures are detected in both optical and X-ray images in 23% of the clusters. This last number may then be considered a lower limit on the fraction of real substructures in clusters, and it is large! Indeed, it implies that one in four clusters may be out of equilibrium due to the presence of a substructure. The dynamical status of individual clusters should therefore be examined in detail before being used in other studies.

In this paper we present a study of the dynamical status of the cluster Abell 970, from the analysis of the positions and velocities of cluster galaxies, as well as from the intra-cluster gas X-ray emission. Abell 970 has a richness class $R = 0$ and type B-M III (Abell, Corwin & Olowin 1989). Together with a few other clusters, (A979, A978 and A993) it is member of the Sextans supercluster (number 88 in the catalogue of Einasto et al. 1997, and number 378 in the catalogue of Kalinkov, Valtchanov & Kuneva 1998). It has a moderate cooling flow (White, Jones & Forman 1997).

A search in NED database¹ indicates that only 4 radial velocities are known in the field of the cluster (see Postman et al. 1992) which, however, have not been published. Here we examine some properties of the cluster Abell 970, using a set of 69 new radial velocities. The observations of radial velocities reported here are part of a program to study the dynamical structure of clusters of galaxies, started some years ago and with several results already published (see *e.g.* Proust et al. 1987, 1988, 1992, 1995, 2000, Capelato et al. 1991).

This paper is organized as follows. We present in Sect. 2 the details of the observations and data reduction. In Sect.s 3 and 4 we discuss the galaxy and the X-ray distributions, respectively. In Sect. 5 we analyze the velocity distribution of the cluster galaxies. In Sect. 6 we present mass estimates for the central region of the cluster, derived from the optical and X-ray observations. In Sect. 7 we discuss the dynamical status of Abell 970. Finally, in Sect. 8 we summarize our conclusions. We adopt here, whenever necessary, $H_0 = 50 h_{50} \text{ km s}^{-1} \text{ Mpc}^{-1}$.

2. Observations and Data Reductions

The new velocities presented in this paper have been obtained with the 1.52m ESO telescope at La Silla (Chile), the 2.0m telescope at Pic du Midi (France), and with the 1.93m telescope at Haute-Provence Observatory (France).

Observations with the 1.52m ESO telescope were carried out in February 1996. We used the Boller and Chivens spectrograph at the Cassegrain focus, equipped with a

¹ The NASA/IPAC Extragalactic Database (NED) is operated by the Jet Propulsion Laboratory, California Institute of Technology, under contract with the National Aeronautics and Space Administration

600 lines/mm grating blazed at 5000 Å and coupled to an RCA CCD detector (1024 × 640 pixels) with pixel size of 15 μm. The dispersion was 172 Å/mm, providing spectral coverage from 3750 to 5700 Å. The exposure times ranged between 30 and 60 minutes, according to the magnitude of the object. During the run, calibration exposures were made before and after each galaxy observation using an He-Ar source.

Observations with the 1.93m Haute-Provence Observatory telescope were carried out in November 1997, November 1998 and April 2000. We used the CARELEC spectrograph at the Cassegrain focus, equipped with a 150 lines/mm grating blazed at 5000 Å and coupled to an EEV CCD detector (2048x1024 pixels) with pixel size of 13.5 μm. The dispersion of 260 Å/mm allowed a spectral coverage from 3600 to 7300 Å. Wavelength calibration was done using exposures of Hg-Ne lamps.

Part of the velocities were obtained during an observing run at the 2.0m Bernard Lyot telescope at Pic du Midi Observatory in January 1997. Despite the declination of Abell 970, we used the ISARD spectrograph in its long-slit mode with a dispersion of 233 Å/mm with the TEK chip (1024x1024 pixels) of 25 μm, corresponding to 5.8 Å/pixel. Typically two exposures of 2700s each were taken for fields across the cluster. Wavelength calibration was done using Hg-Ne lamps before and after each exposure.

Data reduction was carried out with IRAF² using the *longslit* package. The spectra were rebinned uniformly in log wavelength, with a scale of 1 Å/bin. Radial velocities were determined using the cross-correlation technique (Tonry and Davis 1979) implemented in the RVSAO package (Kurtz et al. 1991, Mink et al. 1995), with radial velocity standards obtained from observations of late-type stars and previously well-studied galaxies.

Table 1³ lists positions and heliocentric velocities for 69 individual galaxies in the field of the cluster. The entries of the table are:

1. identification number
2. right ascension (J2000)
3. declination (J2000)
4. morphological type determined from a visual inspection of the Palomar sky survey (POSS) images
5. b_J magnitude from the COSMOS/UKST Southern Sky Object Catalogue
6. heliocentric radial velocity with its error (km s⁻¹)
7. R-value derived from Tonry & Davis (1979)

² IRAF is distributed by the National Optical Astronomy Observatories, which are operated by the Association of Universities for Research in Astronomy, Inc., under cooperative agreement with the National Science Foundation.

³ Table 1 is also available in electronic form at the CDS via anonymous ftp 130.79.128.5.

8. telescope and notes- **e**: 1.52m ESO telescope, **o**: 1.93m OHP telescope; **p** 2.0m Pic du Midi telescope

For the analysis in the next sections is important to estimate the completeness level of the velocity sample as a function of the magnitude. To do that (and also to study the cluster galaxy projected distribution) we extracted from the COSMOS/UKST Southern Sky Object Catalogue, supplied by the Anglo-Australian Observatory (Drinkwater, Barnes & Ellison 1995) a sample of galaxies in the direction of the cluster. An examination of Table 1 indicates that, with one exception, all velocities were measured in a region of $\sim 27' \times 22'$ (in RA and DEC, respectively), centered on the position of galaxy number 1 in Table 1, what assured a good level of completeness in the core of the cluster. Indeed, by comparing the velocity and the COSMOS catalogues we verify that, within this region, our velocity sample is $\sim 92\%$ complete at $b_J^{cosmos} = 18$, $\sim 75\%$ at $b_J^{cosmos} = 19$, and $\sim 51\%$ at $b_J^{cosmos} = 19.75$.

3. Galaxy distribution

We present in Fig. 1 the distribution of galaxies in the direction of Abell 970, obtained from the COSMOS catalogue, for galaxies brighter than $b_J^{cosmos} < 19.75$ (235 objects). The plot is centered on an E/D galaxy (number 1 in Table 1) and has $45' \times 45'$ (i.e., about $4.6 \times 4.6 h_{50}^{-1}$ Mpc). It is interesting to point out that, amongst the cluster galaxies with known velocities, this is the second brightest galaxy ($b_J^{cosmos} = 16.57$).

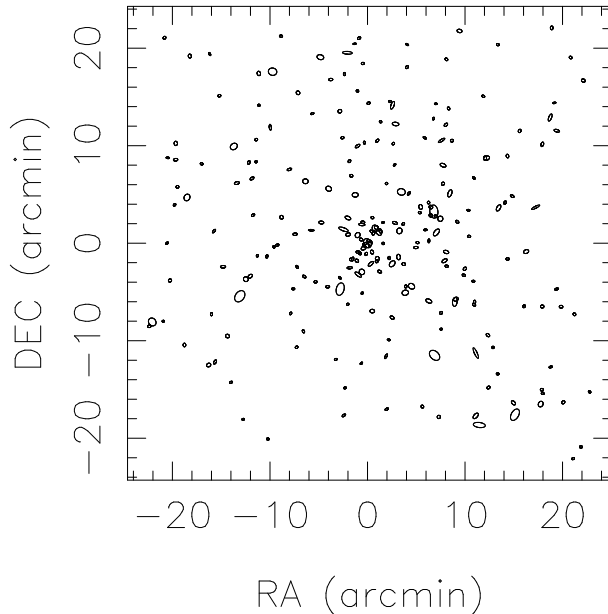


Fig. 1- Galaxies brighter than $b_J^{cosmos} < 19.75$ in the field of Abell 970. The plot is centered on galaxy number 1 in Table 1.

Table 1. Heliocentric redshifts for galaxies.

GALAXY	R.A. (2000)	DEC. (2000)	TYPE	b_J^{cosmos}	VELOCITY $V \pm \Delta V$	R	N
01	10 17 25.7	-10 41 21	E/D	16.57	17525 52	9.72	e
02	10 17 24.6	-10 41 22	S0	18.00	16209 37	7.14	e
03	10 17 28.3	-10 40 59	S0/S	18.67	18424 74	5.48	e
04	10 17 29.7	-10 40 31	S0	17.62	16270 52	9.67	e
05	10 17 26.3	-10 41 34	S0	17.51	18357 54	6.60	e
06	10 17 23.9	-10 42 16	S0/S	18.41	16435 69	5.61	e
07	10 17 27.3	-10 41 51	E/S0	18.36	18145 53	5.89	e
08	10 17 29.5	-10 42 17	S	18.38	17404 71	7.42	e
09	10 17 21.7	-10 42 56	S	17.96	17631 61	6.91	e
10	10 17 24.3	-10 43 29	S	17.95	16341 81	6.76	e
11	10 17 31.8	-10 42 59	S0/S	18.83	17769 81	5.79	e
12	10 17 30.0	-10 43 09	S0	18.45	17327 35	5.57	e
13	10 17 32.9	-10 43 52	S	18.26	16974 36	5.14	e
14	10 17 29.4	-10 44 34	Sa	17.69	18909 75	5.61	e
15	10 17 28.0	-10 44 18	S0	17.67	18030 29	8.46	e
16	10 17 20.7	-10 44 16	S	18.56	17711 26	5.85	e
17	10 17 15.6	-10 43 28	Sa	17.51	19503 96	2.62	e
18	10 17 12.9	-10 42 47	S0	17.83	19450 51	9.10	e
19	10 17 35.6	-10 39 55	Sb	17.15	18789 24	9.41	e
20	10 17 28.1	-10 39 27	Sa	18.16	16842 76	4.79	e
21	10 17 27.6	-10 39 12	S0	18.63	16404 92	4.48	e
22	10 17 21.0	-10 40 13	S0	17.18	18788 45	9.41	e
23	10 17 23.2	-10 40 18	E	18.26	19381 40	10.12	e
24	10 17 22.0	-10 39 45	E	18.00	16847 47	6.37	e
25	10 17 22.5	-10 39 50	E/S0	17.09	19483 54	9.32	e
26	10 17 25.2	-10 41 07	E	18.87	17081 93	3.15	e
27	10 17 28.5	-10 41 13	E	17.52	33586 98	2.84	e
28	10 17 21.9	-10 43 12	E/S0	18.71	17764 64	5.17	e
29	10 17 14.4	-10 39 16	S	18.46	18415 94	3.44	e
30	10 17 12.6	-10 40 05	E/S0	17.69	16533 80	5.36	e
31	10 17 33.6	-10 38 46	SB	17.88	17779 109	4.68	e
32	10 17 44.6	-10 39 14	S0/S	18.09	17992 33	7.55	e
33	10 17 32.4	-10 34 27	S0	19.01	17606 98	2.75	e
34	10 17 30.7	-10 36 24	S	17.43	16722 134	3.55	e
35	10 17 41.6	-10 35 46	S0/S	17.63	21637 37	8.62	e

GALAXY	R.A. (2000)	DEC. (2000)	TYPE	b_J^{cosmos}	VELOCITY $V \pm \Delta V$	R	N
36	10 17 51.1	-10 35 00	E	17.29	16661 62	4.42	e
37	10 17 36.9	-10 46 01	S	16.8 ⁷	11957 79	4.97	e
38	10 17 36.8	-10 46 05	S0/S	16.8 ⁷	12221 77	4.70	e1
39	10 16 55.8	-10 38 51	Sa	17.83	17570 74	7.53	e
40	10 16 58.5	-10 38 07	S0/S	16.42	17184 44	6.33	e
41	10 16 59.7	-10 37 39	E	18.62	17873 59	6.44	e
42	10 17 00.6	-10 37 12	E	19.16	17194 66	5.58	e
43	10 17 03.9	-10 37 38	E/S0	18.11	17690 52	7.14	e
44	10 17 11.8	-10 36 07	E/S0	16.43	21998 84	8.33	e2
45	10 16 57.5	-10 40 16	E	17.46	17903 48	9.11	e
46	10 17 02.0	-10 39 59	E	19.10	18843 98	4.53	e3
47	10 17 07.6	-10 45 46	S0	16.89	17202 86	15.72	e4
48	10 17 10.2	-10 46 26	E/S0	17.13	17475 46	12.24	e5
49	10 16 49.9	-10 47 23	Sb	16.91	17487 64	6.73	e
50	10 17 00.5	-10 47 17	Sa	17.38	21166 107	3.77	e
51	10 16 54.1	-10 43 10	S0/S	18.45	17257 85	4.71	e
52	10 16 53.2	-10 43 43	E	18.83	17351 85	6.70	e
53	10 17 47.0	-10 45 19	S	19.14	16771 138	2.96	p
54	10 18 18.0	-10 46 48	E/S0	15.95	11579 63	8.04	p
55	10 18 15.6	-10 45 03	S0	17.69	12056 81	3.26	p
56	10 17 51.6	-10 44 47	E	19.44	16372 89	2.53	p
57	10 17 54.6	-10 43 47	S0	19.44	45962 93	2.61	p
58	10 18 06.9	-10 42 43	S	19.13	51814 76	2.41	p
59	10 18 04.0	-10 41 44	SBc	19.68	48068 73	3.01	p
60	10 17 57.7	-10 33 48	S	18.52	16228 44	4.53	p
61	10 18 13.0	-10 34 42	S	18.47	11675 69	5.34	o6
62	10 16 55.2	-10 30 49	S	18.16	18371 133	3.30	o
63	10 16 54.7	-10 33 22	S	17.86	17737 75	4.47	o
64	10 16 36.9	-10 32 38	S0	17.58	17982 82	5.62	o
65	10 16 51.9	-10 36 15	S	17.53	18255 84	5.39	o
66	10 16 48.8	-10 39 10	S0	18.67	18293 63	6.48	o
67	10 17 42.0	-10 45 49	E	18.60	12101 114	3.22	o
68	10 16 37.3	-10 32 39	?	18.77	17589 136	3.04	o
69	10 16 41.3	-10 52 38	S	17.37	17649 42	8.74	o

emission lines: **1** [OIII], $H\alpha$, [SII] = 12084 km s^{-1} ; **2** $H\alpha$ = 22087 km s^{-1} ; **3** $H\alpha$ = 18858 km s^{-1} ; **4** $H\alpha$ = 17234 km s^{-1} ; **5** $H\alpha$ = 17523 km s^{-1} ; **6** measured on $H\beta$, [OIII], $H\alpha$. **7** estimated magnitude (see Sect. 4).

The adaptive kernel density map (Silverman, 1986) corresponding to this sample is given in Fig. 2. This figure indicates that the galaxy distribution in the field of Abell 970 is approximately regular, with the projected density peaking at the position of the E/D galaxy. There is a substructure at NW, near galaxy number 40 in Table 1. This is the brightest cluster galaxy (considering only galaxies with known radial velocities); it is classified as S0/S and has magnitude $b_J^{cosmos} = 16.42$. This figure also indicates that the cluster radial extension may attain several Mpc.

It is worth noting that all features displayed in this map are significant. The significance regions are obtained through a bootstrap resampling procedure applied to the sample coordinate distribution. This allows the construction of a map of standard deviations of the projected density. By subtracting the projected density map from the standard deviation map (multiplied by a given number, say 3), we define the *significance regions* of the projected density map as those regions for which the resulting subtracted map is positive.

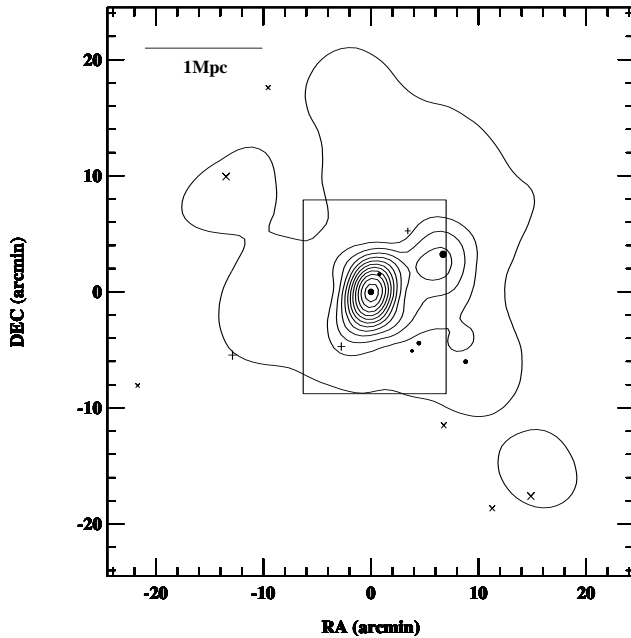


Fig. 2- Projected density map of the galaxies brighter than $b_J^{cosmos} = 19.75$ in the field of Abell 970, together with the positions of the 15 brightest ones. The peak density of this map corresponds to about $210 \text{ galaxies Mpc}^{-2} h_{50}^2$. All density levels in this map are significant. Other symbols are as follows- Dots: galaxies kinematically linked to the cluster; Pluses: galaxies projected in this field but not belonging to the cluster; Crosses: galaxies with no measured velocities. The central rectangle displays the area covered by the X-ray image of Fig. 4.

4. The X-ray emission and the gas distribution

Abell 970 is a X-ray source, first observed with Einstein IPC in June 1980 (Ulmer et al. 1981). It was also observed during the ROSAT all-sky survey (Voges 1992), in 1990, and is included in the X-ray-brightest Abell type cluster catalog (XBACs; Ebeling et al. 1996).

Since Abell 970 had no measured X-ray temperature, Ebeling et al. (1996) determined the X-ray flux, luminosity and temperature using an iterative method running roughly as follows: assuming an initial X-ray temperature of 5 keV, the bolometric luminosity was computed. Then, with this luminosity and using the T_X-L_X relation from White, Forman & Jones (1996), a new estimate of the temperature was made which, in turn, was used to compute a new luminosity and so on. Thus, with Rosat data and the above mentioned T_X-L_X relation, Ebeling et al. (1996) quoted a flux equal to 9.9×10^{-12} erg cm⁻² s⁻¹, luminosity of 1.50×10^{44} erg s⁻¹ (both in the 0.1–2.4 keV band), and gas temperature $kT_X = 3.6$ keV. By applying this same iterative method to the Einstein IPC data, Jones & Forman (1999) derived a X-ray luminosity of 2.13×10^{44} erg s⁻¹ in the [0.5–4.5 keV] band and a bolometric luminosity equal to 3.79×10^{44} erg s⁻¹, which is in accordance with the temperature given by Ebeling et al. (1996). Moreover, White, Jones & Forman (1997), using this same data, suggests that Abell 970 has a weak cooling-flow, with a mass deposition rate $\dot{M} = 20^{+32}_{-20} M_\odot \text{ yr}^{-1}$ (see also Loken, Mellot & Miller 1999).

However, since the Einstein IPC detector had some spectroscopic capability, it is possible to estimate its temperature by a direct fitting of the available spectra. We have thus obtained both the ‘events’ and image (in the 0.2–3.5 keV band, rebinned to 24 arcsec per pixel) files from the HEASARC Online Service. The spectrum of Abell 970 was extracted from the events file with XSELECT and analysed with XSPEC using the PI channels 4–12 (0.5–4.5 keV) within a region of 9.6 arcmin (corresponding to $1 h_{50}^{-1}$ Mpc). The X-ray emission was fitted with a single temperature, absorbed MEKAL model (Kaastra & Mewe 1993; Liedahl et al. 1995). We have also used the recipe given by Churazov et al. (1996) for computing the weights (available in XSPEC), based on the smoothed observed spectrum. With these weights, one can still use the least-square minimisation and the χ^2 statistics to estimate the confidence interval of the fitted parameters.

With only 9 bins covering the 0.5–3.5 keV band, it is impossible to constrain the metallicity. Therefore we have fixed Z to the ‘canonical’ value of $0.3 Z_\odot$, which is the mean value obtained for 40 nearby clusters by Fukazawa et al. (1998). Also, with only 3 bins with energy less than 1 keV, it is difficult to constrain independently the temperature and the hydrogen column density. This happens because they are correlated (e.g. Pislar et al. 1997). Therefore, we have also fixed the hydrogen column density at $N_H = 5.3 \times 10^{20} \text{ cm}^{-2}$,

the galactic value at the Abell 970 position (Dickey & Lockman 1990). Fig. ?? shows the fitting of the X-ray spectrum. The results are summarised in Table 2.

Table 2. X-ray spectral fitting results. kT is the gas temperature, N_{H} is the hydrogen column density, Z is the metallicity, L_X is the [0.5–4.5 keV] non-absorbed luminosity inside $1 h_{50}^{-1}$ Mpc, and the last column gives the χ^2 and number of degrees of freedom. Errors are at a confidence level of 68%.

kT (keV)	N_{H} (10^{20}cm^{-2})	Z (Z_{\odot})	L_X ($10^{44} \text{ergs s}^{-1}$)	χ^2/dof	Notes: * Value fixed. Varying the
$3.1_{-0.6}^{+1.0}$	5.3^*	0.3^*	1.8	6.57/7	

metallicity from 0.1 to $0.5 Z_{\odot}$ produces a change in temperature of less than 0.3 keV, increasing towards $Z = 0.1 Z_{\odot}$.

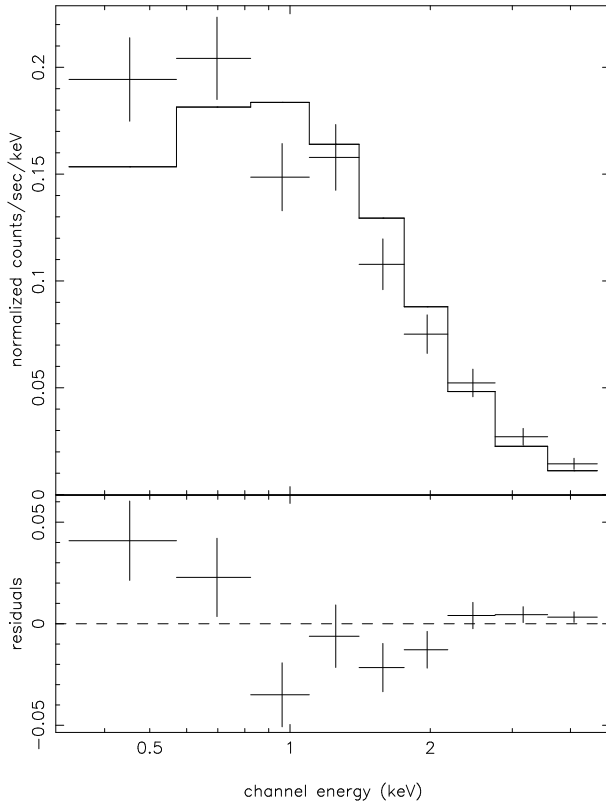


Fig. 3- Fit of the Abell 970 IPC X-ray spectrum. Both the metallicity and hydrogen column density are fixed ($0.3 Z_{\odot}$ and $5.3 \times 10^{20} \text{cm}^{-2}$, respectively).

Although slightly cooler, our temperature is in good agreement with the one derived by Ebeling et al. (1996) and Jones & Forman (1999). Using the σ - T_X relation given by Wu, Xue & Fang (1999), such a temperature corresponds to σ in the range 640–720 km/s.

In Fig. 4 we display the X-ray isophotes of an Einstein IPC image in the [0.2–3.5 keV] band. This image has 24 arcsec per pixel. As it can be seen, the X-ray isophotes are also regular but, interestingly, their peak is not coincident with the peak of the projected density distribution, being slightly displaced towards the substructure associated to the cluster brightest galaxy. Since the relaxation time of the hot gas is expected to be much lower than that of the galaxies, the non-coincidence between the peak of the galaxy distribution and the X-ray emission may be an evidence of a state of non-equilibrium in the galaxy distribution, as expected if the substructure associated to the brightest galaxy has only recently infalled into the cluster. We will explore this point further in next sections. Note that there is not a X-ray emission excess near the substructure detected in the projected density distribution. This is also consistent with the hypothesis that the galaxies in this substructure are members of a group recently captured by the cluster, whose X-ray emission is much lower than that of the cluster.

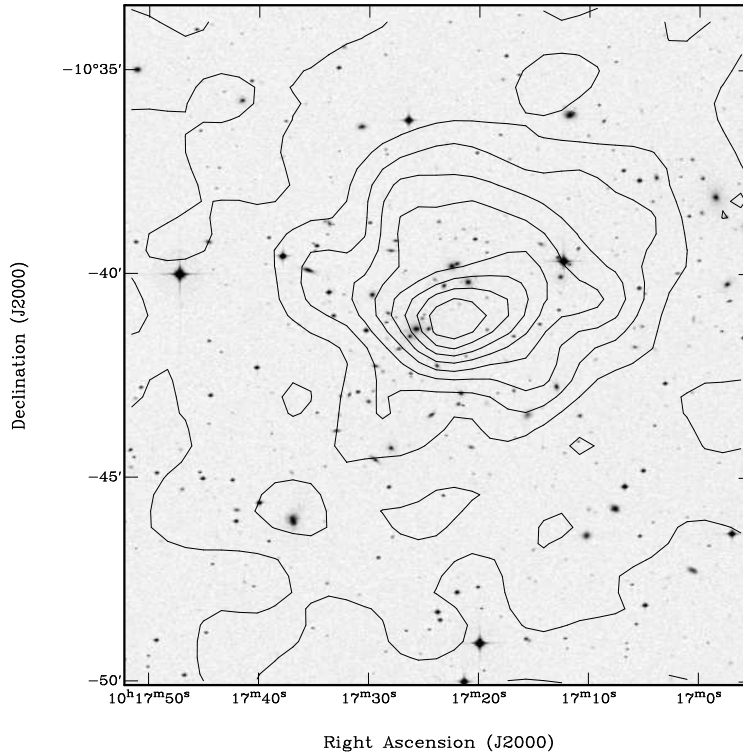


Fig. 4- X-ray isophotes from an Einstein IPC image of Abell 970 (obtained from the HEASARC Online Service) superposed on a DSS image of the cluster.

The X-ray isophotes also show a small peak at SE of the cluster center, at the position of galaxies number 37 and 38 in Table 1, identified in the COSMOS catalogue as just one galaxy with magnitude $b_j^{cosmos} = 16.07$. However, an examination of the optical image of this object using POSS indicates that it indeed corresponds to two merging galaxies. A butterfly-shape due to the tidal currents induced by the merger can be noticed in

the image and the spectrum of object number 38 has emission lines. It is somewhat surprising that this system is not cataloged as an IRAS source. The excess of X-ray emission associated to this galaxy pair may be an evidence of an active nucleus excited by the merger. The magnitudes given in Table 1 were estimated from the COSMOS magnitude assuming that both galaxies have the same luminosity.

5. Velocity analysis

Our sample contains 69 velocities in the direction of Abell 970. Fig. 5 shows a wedge velocity diagram in the direction of the cluster in right ascension (up) and declination (down), and indicates that most of the velocities are between 15000 and 20000 km s^{-1} . A histogram of the velocity distribution of the sample is displayed in Fig. 6. In this section we will discuss the velocity distribution, looking for non-equilibrium effects.

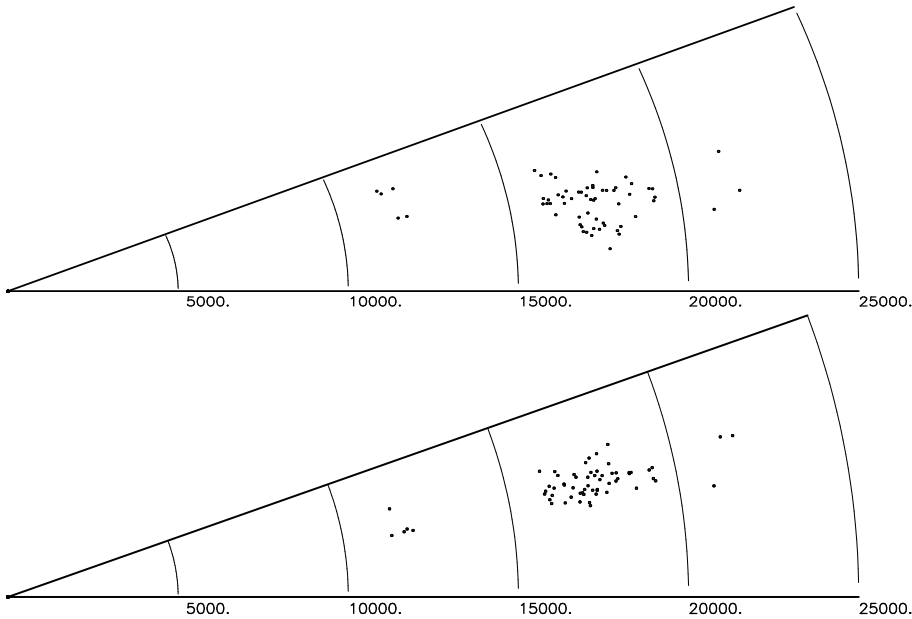


Fig. 5- Wedge velocity diagram in right ascension (up), and declination (down) for the measured galaxies in Abell 970 with radial velocities smaller than 25000 km s^{-1} .

5.1. Normality and dispersion of the velocity distribution

The usual recursive 3σ -clipping (Yahil & Vidal 1977) fails to simultaneously remove the low ($v \sim 12000 \text{ km s}^{-1}$) and high velocity ($v \sim 22000 \text{ km s}^{-1}$) tails of the distribution. We then decided to carefully analyze the radial velocity distribution from the point of view of statistical normality tests, as those provided by the ROSTAT package (Beers et al. 1990; Bird & Beers 1993). With this aim, we have examined several different samples of radial velocities: sample A comprises all galaxies within $11500 \text{ km s}^{-1} < v <$

22000 km s⁻¹; sample *B* is similar to sample *A* without the high- and low-velocity tail, that is 15000 km s⁻¹ < *v* < 20000 km s⁻¹; sample *D* is similar to sample *B* added with the high-velocity tail, that is 15000 km s⁻¹ < *v* < 22000 km s⁻¹; sample *C* contains galaxies within 15000 km s⁻¹ < *v* < 18500 km s⁻¹ and has been considered in view of a significant gap in the data occurring at *v* ~ 18500 km s⁻¹, as indicated by the gap analysis (Wainer & Shacht 1978) provided by ROSTAT.

Table 3 lists the values of the statistics and associated significance levels for the *a*, *u* and *W* tests, which are most sensitive to the tail populations (see discussion in Yahil & Vidal 1977) and the Kolmogorof-Smirnov (KS) normality tests. Only those *p* values significant at levels better than 10% are reported. The other statistical tests provided by ROSTAT have given results always similar to the KS test and so they have been omitted. The last two columns give the values of the Asymmetry Index and the Tail Index (Bird & Beers 1993), which are robust estimators for the skewness and kurtosis of the distribution. The Dip test of unimodality of the distribution also failed to give significant results for any of the samples.

Table 3. Statistics of the velocity distribution.

Sample	N	<i>a</i>	<i>p</i> (<i>a</i>)	<i>u</i>	<i>p</i> (<i>u</i>)	<i>W</i>	<i>p</i> (<i>W</i>)	p(KS)	AI	TI
(1)	(2)	(3)	(4)	(5)	(6)	(7)	(8)	(9)	(10)	(11)
<i>A</i>	65	0.639	0.01	5.005		0.838	0.01	0.01	0.069	1.292
<i>B</i>	56	0.780		3.777	0.02	0.954	0.06		0.081	1.080
<i>C</i>	59	0.711	0.01	4.730		0.881	0.01	0.01	1.057	1.273
<i>D</i>	48	0.829		3.403	0.01	0.940	0.02		-0.514	1.015

The normality hypothesis is rejected for samples *A* and *C* at significance levels better than 3% for all the statistical tests, excepting the *u* test. The values of the statistics of the *a* and *W* tests, as well as the TI values, indicate long tailed underlying distributions. Removing the tails of *A* sample, sample *B*, seems to bring the distribution to normality, as indicated by most of the tests. Although both the *u* and the *W* tests reject normality at high significance levels, their results seem contradictory with the *u* statistics suggesting a cutoff of the underlying distribution while the *W* statistics indicates it is long tailed. Notice that both the AI and TI values are consistent with a normal underlying distribution. Very similar results were obtained for sample *D*, as compared with sample *B*, except that in this case the distribution seems significantly skewed towards low velocities. This is not unexpected for, even if the marginal indication of bimodality of the distribution given by the gap analysis were confirmed, there would be no way, at this level of analysis, to disentangle galaxies belonging to one or to the other underlying distributions. Since

the Dip statistics also fail to reject unimodality, we will not consider this possibility for now and will adopt sample B as representative of the radial velocity distribution of the cluster. We will return to this question at the end of this section.

We will thus assume that the cluster galaxies have radial velocities in the range between 15000 and 20000 km s^{-1} . It is interesting to note that a low velocity tail at $v \sim 12000 \text{ km s}^{-1}$, similar to the one found here, also affected the velocity distribution of the cluster A979 (Proust et al. 1995), which is the nearest neighbor cluster of Abell 970 (at about 3° NE from its center), within the same supercluster. This suggests the existence of a large foreground structure projected in this region of the sky.

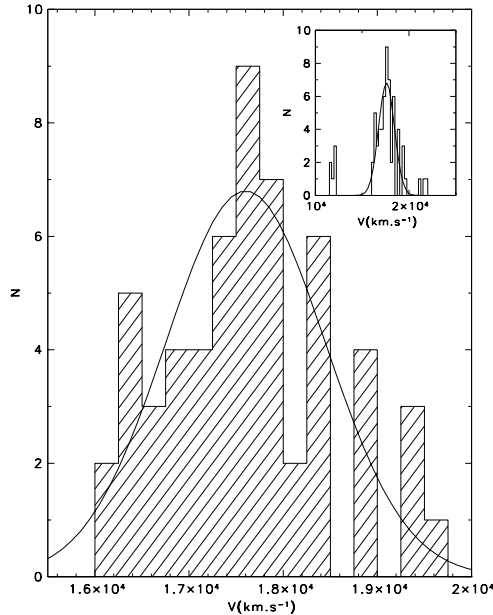


Fig. 6- The radial velocity distribution for the Abell 970 sample of galaxies. The continuous curve shows the Gaussian distribution corresponding to the mean velocity and velocity dispersion quoted in the text (normalized to the sample size and range). The inset displays the velocity distribution between 10000 and 25000 km s^{-1} .

Considering only the 56 galaxies within this velocity range, the cluster mean velocity is $\bar{V} = 17600 \pm 118 \text{ km s}^{-1}$ (corresponding to $z = 0.0587$)⁴. For comparison, the radial velocity of the E/D galaxy located at the center of main cluster is 17525 ± 52 , near that of the whole cluster, as it should be expected if this is the dominant cluster galaxy. The cluster velocity dispersion, corrected following Danese, De Zotti & di Tullio (1980) is $\sigma_{corr} = 845_{-69}^{+92} \text{ km s}^{-1}$ (at a confidence level of 68%). Fig. 6 presents the radial velocity

⁴ In this paper the mean and dispersion velocities are given as biweighted estimates, see Beers et al. (1990).

distribution of the cluster galaxies, as well as a Gaussian curve with the same mean velocity and dispersion observed for these galaxies. Note that this value of σ_{corr} is well above the value favoured by the $\sigma - T_X$ relation, $\sim 700 \text{ km s}^{-1}$ (Sect. 4).

If we consider the morphological types, the mean velocities and corrected velocity dispersions are: $\bar{V} = 17631 \text{ km s}^{-1}$ and $\sigma = 846_{-87}^{+125} \text{ km s}^{-1}$ for $E + S0$ galaxies (35 objects), and $\bar{V} = 17655 \text{ km s}^{-1}$ and $\sigma = 841_{-112}^{+185} \text{ km s}^{-1}$ for $S + I$ galaxies (19 objects). Hence, contrarily to what is observed in most clusters, where the velocity dispersion of the late type population tends to be larger than that of the early type population (Sodré et al. 1989, Stein 1997, Carlberg et al. 1997, Adami et al. 1998), in Abell 970 we do not see any significant difference between the velocity dispersion of these two populations. This might be another indication – besides the presence of a substructure – that Abell 970 is not in overall dynamical equilibrium.

5.2. Substructures in the galaxy distribution

Let us now consider again the substructure, as well as the peak of the galaxy distribution (cf. Fig. 2), taking into account the galaxy velocities. This analysis will be done with galaxies brighter than $b_J^{cosmos} = 19.0$, the magnitude where the completeness of our velocity catalogue in the central regions of the cluster is 75%.

The substructure at NW of the main cluster has, within a 3 arcmin ($274 h_{50} \text{ kpc}$) circular region centered on the brightest S0/S galaxy, 7 cluster galaxies brighter than $b_J^{cosmos} = 19.0$. Together, these galaxies have a low velocity dispersion, $\sigma_{NW} = 378_{-77}^{+120} \text{ km s}^{-1}$, more typical of that of loose groups. The mean velocity is $\bar{V}_{NW} = 17834 \pm 135 \text{ km s}^{-1}$, significantly higher than the overall mean velocity of the cluster. Our velocity catalogue contains 2 galaxies fainter than $b_J^{cosmos} = 19.0$ inside this region. Their inclusion does not significantly change the value of mean velocity, although it increases the velocity dispersion to $\sigma_{NW} = 525_{-87}^{+160} \text{ km s}^{-1}$, a value, however, significantly lower than the cluster overall velocity dispersion. These results are consistent with the suggestion that this clump of galaxies forms a loose group infalling towards the cluster main central condensation. Arguing against the reality of such a group, we notice that its dominant S0/S galaxy is also the lowest velocity member, with $v = 17184 \text{ km s}^{-1}$, but this is not statistically significant.

The central cluster condensation has a N-S elongation (see Fig. 2). A closer examination of the galaxy distribution indicates that this region is dominated by two small clumps of galaxies, which we will denote by A and B (see also Fig. 7 below). Considering circular regions of 1 arcmin ($\sim 91 \text{ kpc } h_{50}^{-1}$), the central clump, A, is tightly concentrated around the E/D galaxy, having 6 galaxies brighter than $b_J^{cosmos} = 19.0$ with $\bar{V}_A = 17624 \text{ km s}^{-1}$, and dispersion $\sigma_A = 816$. The other clump, B, is about 1.5 arcmin NW of clump A and

is more sparse, with only 4 galaxies, of which 3 are tightly packed in velocity space with velocity dispersion $\sigma_B = 711 \text{ km s}^{-1}$ and mean velocity $\bar{V}_B = 19227 \text{ km s}^{-1}$. The fourth galaxy that is, apparently, member of this clump has, however, a very discrepant radial velocity, 16847 km s^{-1} . Since it is not apparent in Fig. 2, it is not clear if B is a real substructure or a fortuitous projected group of cluster galaxies.

5.3. Velocity gradients

Figs 7 and 8 display, respectively, the adaptive kernel maps for the mean velocity and the mean velocity dispersion of the sample of cluster galaxies with measured radial velocities brighter than $b_J^{cosmos} = 18.9$. These maps were calculated from the local kernel weighted averages, with initial kernel size usually larger - in our case by a factor 3, as a compromise between signal-to-noise and spatial resolution - than the optimal size prescribed by Silverman (1986), as suggested by Biviano et al. (1996). Significance regions for each map were obtained by bootstrap, in a fashion similar to that applied to the projected density maps.

The mean velocity map of Fig. 8 clearly indicates the existence of a velocity gradient across the field, roughly in the E-W direction. This occurs because galaxies with $v > 18500 \text{ km s}^{-1}$ populate predominantly the east-side of the field. The mean velocity of the NW group discussed above is consistent with this gradient. Interestingly, this gradient is also consistent with the general gradient one would obtain by considering all galaxies of our catalogue with velocities between 12000 and 22000 km s^{-1} , suggesting that the cluster may be part of a larger structure running more or less in the E-W direction within, at least, this velocity range. In fact a (smaller) velocity gradient, in this same general direction, is also depicted by the mean redshifts of the supercluster members (cf. Einasto et al. 1997).

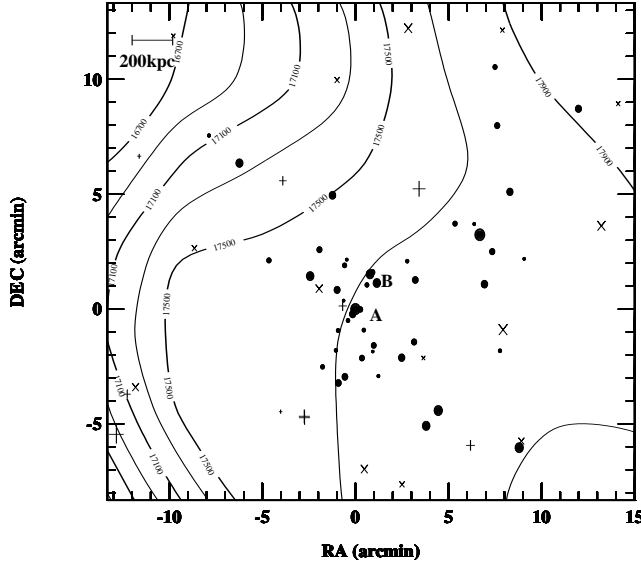


Fig. 7 - Mean velocity map of the galaxies kinematically linked to the cluster and brighter than $b_j^{\text{cosmos}} = 18.9$. The positions of COSMOS galaxies brighter than this limit are also plotted, with symbols following Fig. 3. All regions of this map are significant. A and B correspond to the galaxy clumps discussed in Sect. 5.2.

The mean velocity dispersion map displayed in Fig. 8 indicates that there is a radial gradient of the velocity dispersion. This was confirmed by direct calculations of the velocity dispersions within concentric regions centered in the E/D galaxy. Such a gradient is expected if the cluster grows through the capture of low velocity dispersion groups by the central, main galaxy concentration.

The above discussion points to the complexity of the velocity field of Abell 970. It is possible that the high velocity tail of the cluster velocity distribution displayed in Fig. 6 may be contaminated by another component with mean velocity $\bar{V} \gtrsim 18500 \text{ km s}^{-1}$, which reveals itself by the peculiarities of its spatial distribution. The fact that the velocity distribution shows some signs of bimodality, as pointed out at the beginning of this section, reinforces this suggestion. If real, this component could be interpreted as a diffuse halo located at the East-side of cluster, probably infalling into its dark matter potential well. If correct, such a scenario may be shown up by some X-ray emission features typical of gas shocks produced during this infall.

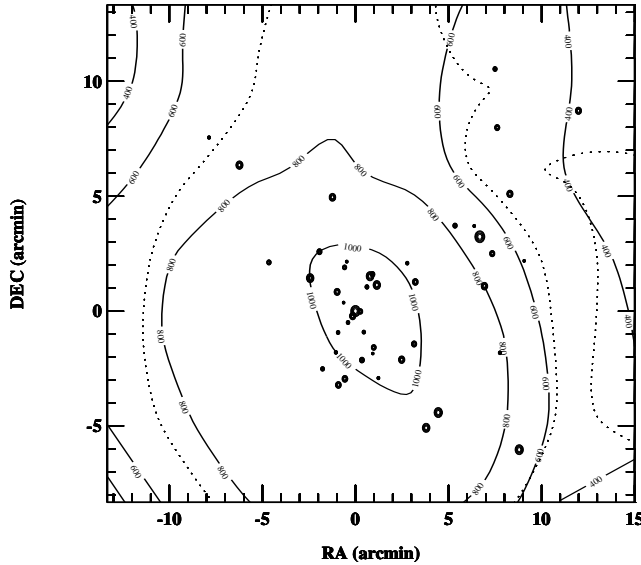


Fig. 8 - Mean velocity dispersion map of the galaxies kinematically linked to the cluster and brighter than $b_J^{\text{cosmos}} = 18.9$. The positions of COSMOS galaxies brighter than this limit are also plotted, with symbols following Fig. 2. The dashed contours delineate the boundaries of the 99% significance levels regions of the map.

6. Cluster mass

In this section we present mass estimates for Abell 970. We first consider the mass derived from its X-ray emission and then we present masses computed from the velocity and galaxy distributions.

6.1. X-ray mass

Supposing that the gas is isothermal, in hydrostatic equilibrium and spherically distributed, the dynamical mass inside r is given by:

$$M(r) = -\frac{kT_X r}{G\mu m_p} \frac{d \log \rho(r)}{d \log r}, \quad (1)$$

where μ is the mean molecular weight ($\mu = 0.59$ for a fully ionized primordial gas) and m_p is the proton mass. If we assume that the gas is described by a β -model,

$$\rho(r) = \rho_0(1 + (r/r_c)^2)^{-3\beta/2}, \quad (2)$$

the dynamical mass becomes:

$$M(r) = 6.68 \times 10^{10} \frac{\beta T_X}{\mu} \frac{r^3}{r^2 + r_c^2} M_\odot, \quad (3)$$

with r and r_c measured in kpc and T_X in keV.

Furthermore, if we have the density contrast $\delta = \bar{\rho}(r)/\rho_c$ (where $\bar{\rho}(r)$ is the mean density inside the radius r and ρ_c is the critical density at the redshift of the cluster) then we can define r_δ as

$$\left(\frac{r_\delta}{r_c}\right)^2 = \frac{5.75 \times 10^7}{\delta h^2 f^2(z, \Omega_0, \lambda_0)} \frac{\beta T_X}{\mu r_c^2}, \quad (4)$$

where $f(z, \Omega_0, \lambda_0)$ depends on the cosmological parameters:

$$f^2(z, \Omega_0, \lambda_0) = \lambda_0 + \Omega_0(1+z)^3 - (\Omega_0 + \lambda_0)(1+z)^2. \quad (5)$$

When $\delta = 200$ we have the usual r_{200} radius, which is about the virial radius, r_{vir} (e.g. Lacey & Cole 1993).

In order to apply the above formulae, we need the parameters for the β -model that describe the intra-cluster gas. We estimate these parameters using the correlations presented by Jones & Forman (1999) between both β and r_c with T_X (Figs. 6 and 7 in their paper). Taking $T_X = 3.1$ keV, we have $\beta \approx 0.5$ and $r_c \approx 100$ kpc. Therefore, we obtain $r_{200}/r_c = 16.2$ or $r_{200} = 1620$ kpc. The corresponding mass is $M(r_{200}) = 2.84 \times 10^{14} M_\odot$. This result agrees well with the virial mass–temperature of Horner, Mushotzky & Scharf 1999 (cf. their Fig. 1 and Table 1). The total mass in the region where the velocities have been measured is $M(r = 1.2h_{50}^{-1}\text{Mpc}) = 2.07 \times 10^{14} M_\odot$.

6.2. Optical Virial Mass

In Fig. 9 we show the cluster mass profile computed with the virial mass estimator (VME) which, as discussed by Aceves & Perea (1999), gives the less biased mass estimates when the system is not completely sampled. These authors also show that the VME overestimates the real mass by no more than 20% at small radii, being more reliable at larger apertures. The error bars in Fig. 9 are 1- σ standard deviations computed using the bootstrap method. The VME assumes, of course, that the system is virialized. In general, the presence of substructures or large scale flows tend to increase the velocity dispersion of the galaxies, leading to an overestimation of the mass of the system.

The VME of Abell 970, within $1.2 h_{50}^{-1}$ Mpc, is $M = (6.80 \pm 1.34) \times 10^{14} M_\odot$, where the error, as before, was computed with the bootstrap method. Note that, for a virialized cluster, these are lower limits for the mass, since we have velocities only for the central region of the system. Indeed, assuming a relation between virial radius and velocity dispersion similar to that adopted by Girardi et al. (1998), we estimate that $r_{\text{vir}} \sim 3.4h_{50}^{-1}$ Mpc, while the velocities have been measured within a region of radius $\sim 1.2h_{50}^{-1}$ Mpc.

Fig. 9 also displays the run of the total b_j luminosity of the cluster (up to $b_j = 19.75$). Considering the VME masses, we find that the mass-luminosity ratio range from 1360 at the cluster central region, to ~ 450 at the largest aperture.

The mass profile derived from the X-ray emission is also presented in Fig. 9. The VME masses are in excess to the X-ray mass estimates by large factors, ranging from ~ 16 for the central apertures, to about 4 at $\sim 1.3 h_{50}^{-1}$ Mpc aperture, which encompasses the whole velocity sample. These factors are well above the uncertainties discussed above for virialized clusters. In fact, the dynamical mass determined by the X-ray emission at radius $r \gg r_c$ depends essentially on the temperature and the asymptotical slope of the gas density. Both are ill determined with the available data; it is then possible that one of them (or both) are under-estimated, which implies that we under-estimate the dynamical X-ray mass. For instance, if β is as high as 0.75 and $T_X = 4.1$ (cf. the error bars in Table 2), then the dynamical X-ray mass would be twice the estimated value, i.e., $M(r = 1.2h_{50}^{-1}\text{Mpc}) = 4.1 \times 10^{14} M_{\odot}$. On the other side, the presence of a substructure associated to the cluster brightest galaxy, as well as the mean velocity gradient, may be an indication of non-virialization and, consequently, the VME may be largely overestimated.

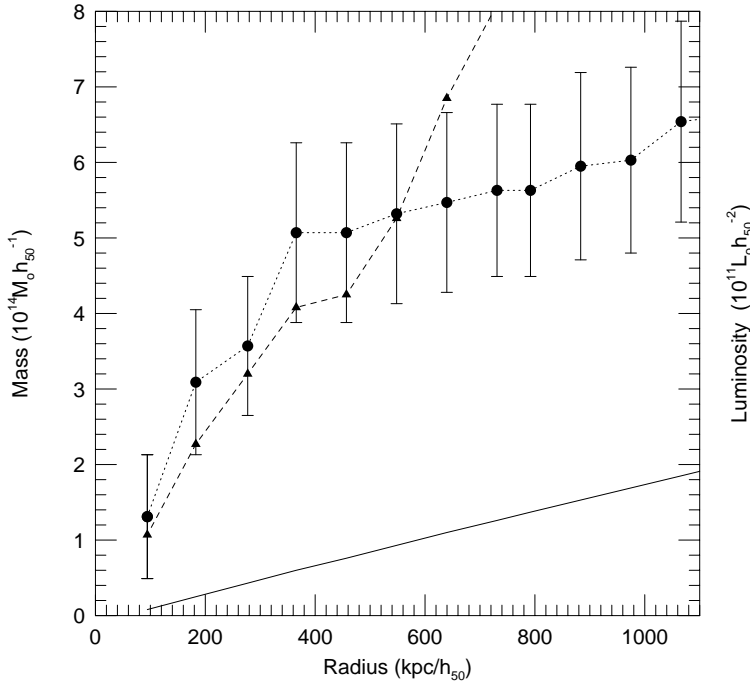


Fig. 9 - Cluster optical masses (circles and dotted lines) and luminosities (triangles and dashed lines). The X-ray masses are given by the continuous line. Filled symbols give estimates using the whole sample of velocities.

7. The dynamical status of Abell 970

Several evidences indicate that Abell 970 is not in an overall state of virialized equilibrium. Indeed, the presence of a substructure at NW of the main galaxy concentration may indicate that the cluster has been capturing groups of galaxies of its neighborhood. The large scale gradient in the mean velocity of the galaxies, shown in Fig. 8, is also not expected in virialized systems. Other evidences for non-equilibrium include the discrepancy in the peaks of the X-ray emission and of the galaxy projected density, and the observed differences between optical and X-ray masses.

Accordingly to Allen (1998), there is a good agreement between X-ray and strong gravitational lensing mass measurements only in clusters with strong cooling flows; in clusters with modest or absent cooling flows, the masses determined from the X-ray data are 2 to 4 times smaller than the masses estimated from strong gravitational lensing. The reason for the mass discrepancy is the dynamical status of the central regions of the clusters: those with strong cooling flows are relaxed and virialized, while those with small cooling flows are out of the equilibrium, and the assumption of hydrostatic equilibrium that underlies the X-ray mass estimates is not valid. Indeed, the presence or absence of cooling flows can be used as a diagnostic to verify whether galaxy clusters are in dynamical equilibrium in their central regions. Abell 970 has at most a weak cooling flow, of $\dot{M} = 20^{+32}_{-20} M_{\odot} \text{ yr}^{-1}$ (Ebeling et al. 1996), and our results, indicating that this system is not relaxed, are consistent with the findings of Allen (1998).

It is interesting to note that the offset between the X-ray and galaxy distribution centers, although significant, is not very large. It is possible that Abell 970 had a much stronger cooling flow until recently, that was interrupted by dynamical perturbations induced by the arrival of a galaxy group (now observed as a substructure) in the central regions of the cluster. Given that in the cluster densest regions the gas relaxes very quickly, compared with the time the galaxy distribution takes to achieve equilibrium, it is natural to think of cooling flows as an intermittent process, that is disrupted by dynamical perturbations and that resumes activity after the relaxation is achieved. The time scale of intermittency, in this scenario, depends strongly on the accretion rate of groups by the cluster.

8. Summary

In this paper, we have presented an analysis of the galaxy cluster Abell 970, based on a new set of radial velocities and on X-ray observations. The study of the galaxy projected positions reveals a relatively regular distribution, centered on an E/D dominant galaxy. The analysis with the adaptive kernel density map indicates the presence of a statistically significant substructure at NW of the cluster main galaxy concentration, centered on a

S0/S galaxy that is the brightest cluster member. The X-ray emission distribution does not reveal any emission excess due to that substructure but, interestingly, the peak of the X-ray emission is not coincident with the cluster center (at the position of the dominant galaxy), being displaced towards the direction of the substructure. These results suggest that this substructure is real and that the cluster may not be in an overall state of dynamical equilibrium.

Further evidence that the cluster is in a state of non-equilibrium comes from the analysis of the radial velocity distribution. For instance, the cluster velocity dispersion, 845 km s^{-1} (increasing to $\sim 1000 \text{ km s}^{-1}$ at the cluster center), is significantly larger than the value expected from the $\sigma - T_X$ relation, that is $\sim 700 \text{ km s}^{-1}$. Also, the substructure detected in the galaxy projected distribution has a much smaller velocity dispersion, 381 km s^{-1} , that is typical of loose groups. Together, these results suggest that this substructure may be a group that have recently arrived in the central regions of the cluster. The presence of large scale velocity gradients is another evidence that Abell 970 is out of equilibrium. The virial mass of this cluster is much larger than the mass inferred from the X-ray emission. This discrepancy is indeed expected if the underlying hypothesis of these mass estimators, namely that galaxies and gas inside the cluster are in hydrostatic equilibrium, is not actually fulfilled.

The fact that Abell 970 has a dim cooling flow also fits nicely in the above scenario if, as suggested by Allen (1998), only clusters in equilibrium exhibit massive cooling flows. Indeed, cooling flows may have an intermittent behavior: phases of massive cooling flows may be followed by phases without significant cooling flows after the accretion of a galaxy group massive enough to disrupt the dynamical equilibrium in the center of the clusters. After a new equilibrium is achieved, a massive cooling flow will be established again. Hence, in hierarchical scenarios for structure formation, intermittent cooling-flows should be an usual phenomenon.

Acknowledgements. We thank the OHP, Pic du Midi and ESO staff for their assistance during the observations, and especially Gilles Charvin, student at the Ecole Normale Supérieure de Lyon for his valuable scientific collaboration. LSJ, HVC, GBLN and HC thank the financial support provided by FAPESP, CNPq and PRONEX. DP acknowledges support from ECOS/CONICYT project C96U04. This research has made use of data obtained through the High Energy Astrophysics Science Archive Research Center Online Service, provided by the NASA/Goddard Space Flight Center.

References

- Abell G.O., Corwin H.G., Olowin R.P., 1989, ApJSS 70, 1
 Adami C., Biviano A., Mazure A., 1998, A&A 331, 439
 Allen S. W., 1998, MNRAS 296, 392

- Aceves H., Perea J., 1999, *A&A* 345, 439
- Bahcall N.A., Fan X., 1998, *ApJ* 504, 1
- Biviano A., Durret F., Gerbal D., le Fevre O., Lobo C., Mazure A., Slezak E., 1996, *A&A* 311, 95
- Beers T. C., Flynn K., Gebhardt K., 1990, *AJ* 100, 32
- Bird C. M., Beers T. C., 1993, *AJ* 105, 159
- Capelato H.V., Mazure A., Proust D., Vanderriest C., Lemonnier J.P., Sodré L., 1991, *A&AS* 90, 355
- Carlberg R.G., Yee H.K.C., Ellingson E., 1997, *ApJ* 478, 462
- Churazov E., Gilfanov M., Forman W., Jones C., 1996, *ApJ* 471, 673
- Danese L., De Zotti G., di Tullio G., 1980, *A&A* 82, 322
- Dickey J.M., Lockman F.J., 1990, *ARA&A* 28, 215
- Drinkwater M.J., Barnes D.G., Ellison S.L., 1995, *PASA* 12, 248
- Einasto M., Tago E., Jaaniste J., Einasto J., Andernach H., 1997, *A&AS* 123, 119
- Fukazawa Y., Makishima K., Tamura T., Ezawa H., Haiguang X., Ikebe Y., Kikuchi K., Ohashi T., 1998, *PASJ* 50, 187
- Girardi M., Giuricin G., Mardirossian F., Mezzetti M., Boschin W., 1998, *ApJ* 505, 74
- Horner D., Mushotzky R.F., Scharf C.A., 1999, *ApJ* 520, 78
- Irwin J.A., Bregman J.N., Evrard A.E., 1999, *ApJ* 519, 518
- Kaastra J.S., Mewe R., 1993, *A&AS* 97, 443
- Kalinkov M., Valtchanov I., Kuneva I., 1998, *A&A* 331, 838
- Kauffmann G., Colberg J.M., Diaferio A., White S.D.M., 1999, *MNRAS* 303, 188
- Kolokotronis V., Basilakos S., Plionis M., Georgantopoulos I., 2000, preprint (astro-ph/0002432)
- Kurtz M.J., Mink D.J., Wyatt W.F., Fabricant D.G., Torres G., Kriss G.A., Tonry J.L., 1991, *ASP Conf. Ser.* 25, 432
- Lacey C., Cole S., 1993, *MNRAS* 262, 627
- Lacey C., Cole S., 1994, *MNRAS* 271, 676
- Lanzoni B., Mamon G.A., Guiderdoni B., 2000, *MNRAS* 312, 781
- Liedahl D.A., Osterheld A.L., Goldstein W.H., 1995, *ApJ* 438, L115
- Loken C., Melott A.L., Miller C.J., 1999, *ApJ* 520, L5
- Mellier Y., 1999, *ARA&A* 37, 127
- Mink D.J., Wyatt W.F., 1995, *ASP Conf. Ser.* 77, 496
- Mushotzky R.F., Loewenstein M., Arnaud K., Fukazawa Y., 1995, in *Dark Matter*, ed. S.S. Holt & C.L. Bennett (New York: AIP), page 231
- Postman M., Huchra J.P., Geller M.J., 1992, *ApJ* 384, 404
- Postman M., Lauer T.R., 1995, *ApJ* 440, 28
- Press W. H., Schechter P., 1974, *ApJ* 187, 425
- Proust D., Talavera A., Salvador-Solé E., Mazure A., Capelato H.V., 1987, *A&AS* 67, 57
- Proust D., Mazure A., Sodré L., Capelato H., Lund G., 1988, *A&AS* 72, 415
- Proust D., Quintana H., Mazure A., de Souza R., Escalera E., Sodré L., Capelato H.V., 1992, *A&A* 258, 243

- Proust D., Mazure A., Vanderriest C., Sodré L., Capelato H.V., 1995, *A&AS* 114, 565
- Proust D., Cuevas H., Capelato H.V., Sodré L., Tomé Lehodey B., Le Fèvre O., Mazure A., 2000, *A&A* 355, 443
- Richstone D., Loeb A., Turner E.L., 1992, *ApJ* 393, 477
- Sodré L., Capelato H.V., Steiner J.E., Mazure A., 1989, *AJ* 97, 1279
- Stein P., 1997, *A&A* 317, 670
- Tonry J., Davis M., 1979, *AJ* 84, 1511
- Ulmer M.P., Kowalski M.P., Cruddace R. G., Johnson M., Meekins J., Smathers H., Yentis D., Wood K., McNutt D., Chubb T., Byram E.T., Friedman H., 1981, *ApJ* 243, 681
- Voges W., 1992, The ROSAT All-Sky X-ray Survey, in: *Proceedings of Satellites Symposium 3*, ESA, ISY-3, p. 9
- Wainer H., Shacht S., 1978, *Psichometrika* 43, 203
- White D.A., Jones C., Forman W., 1997, *MNRAS* 292, 419
- Wu X.P., Chiueh T., Fang L.Z., Xue Y.J., 1998, *MNRAS* 301, 861
- Wu X.P., Xue Y.J., Fang L.Z., 1999, *ApJ* 524, 22
- Yahil, A. and Vidal, N.V., 1977, *ApJ*, 214, 347